

# Shear and elongational flow behavior of acrylic thickener solutions

## Part I: Effect of intermolecular aggregation

Saeid Kheirandish · Ilshat Guybaidullin ·  
Wendel Wohlleben · Norbert Willenbacher

Received: 4 February 2008 / Accepted: 26 April 2008  
© Springer-Verlag 2008

**Abstract** We investigate the effect of hydrophobic aggregation in alkali-swellable acrylic thickener solutions on shear and extensional flow properties at technically relevant polymer concentrations using the commercial thickener Sterocoll FD as model system. Apparent molecular weight of aggregates in water is  $M_w \approx 10^8$  g/mol and decreases by more than an order of magnitude in ethanol. Zero shear viscosity  $\eta_0$  is low and shear thinning is weak compared to the high molecular weight of the aggregates. Linear viscoelastic relaxation is described by the Zimm theory up to frequencies of  $10^4$  rad/s, demonstrating that no entanglements are present in these solutions. This is further supported by the concentration dependence of  $\eta_0$  and is attributed to strong association within the aggregates. Extensional flow behavior is characterized using the capillary break-up extensional rheometry technique including high-speed imaging. Solutions with  $\phi \geq 1\%$  undergo uniform deformation and show pronounced strain hardening up to large Hencky strains. Elongational relaxation

times are more than one order of magnitude lower than the longest shear relaxation times, suggesting that aggregates cannot withstand strong flows and do not contribute to the elongational viscosity.

**Keywords** Steady shear · Oscillatory squeeze flow · Elongational flow · CaBER · Acrylate thickener

## Introduction

A broad variety of technically or commercially relevant materials like coatings, adhesives, pharmaceuticals, or personal care products are formulated as complex, multiphase fluids. Besides the liquid continuous phase, these formulations include solid components like inorganic pigments and fillers or organic binder particles, droplets of immiscible fluids, and active ingredients. However, their flow behavior is often controlled by so-called rheology control agents or thickeners in order to provide the desired processing and application properties.

In many technical processes, fluids are subject to complex flow fields incorporating strong extensional components. This is true not only for industrial coating techniques like spraying, curtain coating, or blade coating, but also in filtration operations, fiber spinning, food processing, inkjet printing, and application of personal care, crop protection products, or detergents. Accordingly, not only shear but also extensional flow properties of the corresponding complex formulations have been investigated intensively with respect to processing or application properties. For example, the effect of extensional viscosity on droplet formation and droplet size distribution has been investigated for crop

---

S. Kheirandish · N. Willenbacher (✉)  
Institut of Mechanical Process Engineering and Mechanics,  
University of Karlsruhe, 76128 Karlsruhe, Germany  
e-mail: Norbert.Willenbacher@mvm.uni-karlsruhe.de

*Present Address:*  
S. Kheirandish  
Borealis Polyolefine GmbH, St.-Peters Str. 25,  
4021 Linz, Austria

I. Guybaidullin · W. Wohlleben  
BASF SE, Polymer Research,  
67076 Ludwigshafen, Germany

protection formulations (Dexter 1996) and water-borne coatings (Fernando et al. 2000). Even quantitative relationships between effective elongational viscosity and resulting droplet diameter have been derived for different spray valve geometries and atomization conditions (Stelter et al. 2000, 2002). Extensional flow properties of paper coating colors have been characterized with respect to their impact on coat weight (Kokko et al. 1999) and misting behavior (James et al. 2003). Extensional flow properties determine the atomization of jet fuels (Chao et al. 1984) and the control of precise droplet deposition in inkjet printing (Agarwal and Gupta 2002; Tuladhar and Mackley 2008).

Nevertheless, the determination of the elongational viscosity of low viscosity fluids (like coatings, inks, adhesives, or personal care products) with typical viscosity values in the range of 10–1,000 mPa s is still an experimental challenge. Various techniques like porous media flow, opposing jet rheometry, four-roll mills, entrance pressure loss measurements in capillary rheometry including converging channel flow or bubble growth and collapse measurements have been employed so far (Macosko 1994). These different techniques cover different strain rate and viscosity ranges, but in general the flow kinematics is not purely extensional. The flow can be temporally or spatially inhomogeneous, and only apparent extensional viscosities can be determined, comparison of data using different experimental techniques have to be compared cautiously (Ferguson et al. 1997). In filament-stretching experiments (McKinley and Sridhar 2002), a constant strain rate is imposed on the fluid and the corresponding tensile stress is measured. Under certain constraints, the fluid forms a slender cylindrical filament of uniform thickness, which is uniaxially stretched, and the extensional viscosity can be determined as a function of strain rate and total strain. However, this technique is typically used for fluids in the viscosity range well above 1 Pa s (Bhardwaj et al. 2007; Tripathi et al. 2006).

In this work, we use another filament-thinning technique, namely the capillary break-up extensional rheometry (CaBER; Entov and Hinch 1997; Bazilevskii et al. 2001), in order to characterize the elongational flow properties of aqueous thickener solutions of alkali-swelling acrylate ester copolymers from emulsion polymerization. In a CaBER experiment, a fluid drop is exposed to an extensional step strain, thus forming a liquid filament. Subsequent necking of that liquid bridge is controlled by the balance of capillary and viscoelastic forces. Large extensional strains are attained as the filament undergoes thinning and finally breaks. The only measured quantity is usually the change in

the midpoint diameter with time. The advantage of this method is its wide applicability to various kinds of fluids with low viscosities below 100 mPa s. However, neither strain rate nor stress can be controlled externally, but often very high total strains can be achieved. Various polymer solutions have been investigated using this technique all forming uniform cylindrical filaments, which homogeneously thin and finally break (Stelter et al. 2000, 2002; Clasen et al. 2006a, b; Bhardwaj et al. 2007). In these cases, the tensile stress is directly related to the surface tension of the fluid, the strain rate is defined by the change in the filament diameter, and finally the extensional viscosity can be extracted as a function of total strain. On the other hand, even Newtonian fluids (McKinley and Tripathi 2000) and also many commercially relevant complex fluids like paper coating colors, adhesives, or cosmetic emulsions exhibit non-uniform liquid bridges resulting in a filament shape with concave curvature. In these cases, the calculated viscosity data are transient and/or apparent values (Willenbacher 2004).

Polymers and polyelectrolytes are widely used as thickeners for aqueous formulations (Braun and Rosen 2000). The dependence of extensional viscosity on polymer concentration and molecular weight has been studied for various synthetic (polyethylene oxide, polyacrylamide) and natural polymeric thickeners (xanthan, guar gum) revealing a distinct difference between flexible and stiff polymers. For the latter transient extensional viscosity is lower, strain hardening is less pronounced (Dexter 1996), and at similar relaxation times, their extensional viscosity is lower compared to flexible polymers (Stelter et al. 2002). Systematic data for the shear and elongation rate dependence of the apparent Trouton ratio of cellulose solutions are also available (Kennedy et al. 1995). The characteristic relaxation time of cellulose solutions in filament-thinning experiments was found to be strongly determined by the high molecular weight components and scales with the  $(z + 2)$ -average of the molecular weight distribution (Plog et al. 2005). Systematic studies regarding the effect of elasticity on the extensional flow properties of polymer solutions have been performed using Boger fluids (Ng et al. 1996; Solomon and Muller 1996), and it could be shown that even low concentrations of high molecular weight polymers can cause strong strain hardening and yields Trouton ratios  $\gg 3$ .

The current work focuses on the class of acrylate ester copolymers synthesized in a classical emulsion polymerization process and accordingly supplied as highly concentrated, milky, aqueous dispersions (pH = 2–3.5). Typically, methacrylic acid (MAA), acrylic acid

(AA), and lower acrylates like ethylacrylate (EA) are the main monomers used in commercial applications (Hager and Martin 1957; Miller 1960). These thickeners are widely used in all kinds of water-borne coating or adhesive formulations adjusted to pH values between 7 and 9. Upon neutralization, the weak acrylic or methacrylic acid groups dissociate, thus solubilizing the polymer and developing their thickening properties (Siddiq et al. 1999). These thickeners are often termed alkali-swellaible emulsion polymers (ASE). Their hydrophobically modified (HASE) counterparts belong to the so-called associative thickeners which tend to form aggregates in aqueous solution. The rheological behavior of these systems is therefore strongly controlled by the hydrophobic alkyl groups grafted onto the polymer backbone.

The shear rheological properties of these HASE-type thickeners have been studied intensively (English et al. 1997; Abdala et al. 2004), mainly focusing on the effect of chain length and concentration of the hydrophobic side groups, but also on the backbone composition as well as overall concentration and molecular weight of the polymer. The aggregation of side chains has been proven by fluorescence spectroscopy (Kumacheva et al. 1996). The strong shear-thinning behavior of HASE-type polymer solutions is attributed to the breakup of the side chain aggregates. In transient extensional flow experiments, a pronounced maximum of the elongational viscosity as a function of strain rate is reported, and the viscosity drop at high strain rates is again attributed to the breakup of hydrophobic side chains of the aggregates (Kennedy et al. 1995; Tan et al. 2000).

Even in the absence of grafted hydrophobic side chains, aggregation of polymer chains is an issue for these acrylic thickeners. These materials are assumed to be statistical copolymers (e.g., EA and AA monomers), and if the EA blocks are long enough they get “sticky” or “blocky” and can cause intra- as well as intermolecular association. Accordingly, the existence of large supramolecular aggregates has been clearly observed by static as well as dynamic light scattering experiments (Dai et al. 2000; Wang et al. 2005). The unusual concentration dependence of the shear modulus  $G^*$  also suggested the relevance of aggregation for the thickening properties of ASE-type polymers (Ng et al. 2001). The scope of this paper is to compare shear and elongational flow properties of ASE-type thickener solutions. In part I, we focus on the aggregation phenomenon, which is tightly related to the solvent quality. The forthcoming second part deals with the effect of crosslinking on shear and extensional flow properties.

## Experimental

### Materials

Sterocoll® FD (BASF SE, Ludwigshafen Germany) is an alkali-swellaible thickener for paper coating with moderate thickening power. It is supplied as a highly concentrated, milky, aqueous dispersion with a solids content of 25%, pH of 2.2–2.6 and is based on copolymer of ethylacrylate and (meth)acrylic acid with molar ratio of acrylate to acids of about 1:1.

Field flow fractionation (FFF) has been used to determine the molecular weight of Sterocoll FD dissolved in water as well as ethanol. FFF separates according to the hydrodynamic diameter in the range of 5 to 500 nm, corresponding to molar masses in the range  $3 \times 10^3$  to  $10^8$  g/mol. This technique is widely used for analytical fractionation and determination of molar masses for colloids like lattices, polymers, and agglomerates. The main applications are cationic polyelectrolytes for paper manufacturing or flocculation agents in water treatment (Giddings 1993; Cölfen and Antonietti 2000).

The following experimental set-up has been used here: the separation device is a flat channel (Consensus) about 0.35 mm high, 20 mm wide (conically shaped due to the asymmetric cross-flow), and 300 mm long. One flat side consists of a semipermeable membrane (Amicon YM 10), where a constant part of the carrier liquid is flowing through. Here we use a linearly ramped cross-flow of 0.05–0 ml/min. This cross-flow establishes a concentration gradient that is counteracted by diffusion. Smaller colloidal polymers have higher diffusion coefficients, such that they experience the faster elution flow towards the center of the flow channel. Typical migration times in the channel are 1–40 min (elution flow 0.5 ml/min). Detection by refractive index and multi-angle laser light scattering (Wyatt, Dawn Eos and R.I Optilab DSP) allows simultaneous determination of the distributions of absolute molar mass and radius of gyration. For FFF measurements, solutions were diluted to a concentration of 0.5 g/L in 0.1 N NaNO<sub>3</sub> at pH = 9.5–10. For static light scattering, samples were diluted to a concentration series with 0.01–0.05 g/L in 0.1 N NaNO<sub>3</sub> at pH = 9.5–10 and ethanol, respectively. Independently determined refractive index increments of  $dn/dc = 0.149$  mL/g against water and  $dn/dc = 0.185$  mL/g against ethanol were used for data evaluation. In all cases samples were purified using a 1.2- $\mu$ m cellulose filter. Filtering is essential for FFF in order to remove dust and micron-sized impurities. These would elute in ‘steric mode’ from the FFF channel and would mask the signal from the thickener.

$\text{NaNO}_3$  is a standard non-aggressive salt in the FFF apparatus that partially screens the charges of the polyelectrolyte and thus reduces the inter- and intramolecular electrostatic interactions. The fractionation mechanism of the FFF channel is then a function only of the hydrodynamic diameter, as desired for the determination of molar mass distributions.

From static light scattering, we obtain  $M_w = 0.71 \times 10^8$  g/mol determined in the concentration range 0.01–0.05 g/L. In addition, light scattering yields an average radius of gyration of 275 nm. FFF yields  $M_w = 1.2 \times 10^8$  g/mol in aqueous solution and  $M_w = 4.6 \times 10^6$  g/mol in ethanol both measured at a concentration of 0.5 g/L. These FFF results directly prove the existence of aggregates in aqueous solution and their breakup in ethanol, which is attributed to an improved solubility of the EA sequences.

Solutions of Sterocoll FD prepared for rheological measurements were stirred at room temperature for 48 h and adjusted to the desired pH by slowly adding 1 N NaOH. Polymer concentration was determined thermo-gravimetrically after neutralization. Subsequently, samples were equilibrated for at least 24 h prior to testing. No further change of pH and viscosity was observed within 3 months.

## Methods

### Rotational rheometry

A rotational rheometer Haake RS100 (Thermo Electron) equipped with a cone-plate measuring cell (diameter  $d = 40$  mm, cone angle  $\alpha = 0.01$  rad) was used to perform steady shear as well as small amplitude oscillatory shear experiments. The latter experiment covered the frequency range from 0.01 to 100 rad/s. Strain sweeps at  $\omega = 3.14$  rad/s were performed prior to each frequency sweep in order to identify the linear viscoelastic response regime. All oscillatory shear experiments were performed in a stress-controlled mode and the critical stress of transition from linear to non-linear response varied between 0.2 and 1 Pa, depending on polymer concentration. This corresponds to critical strain amplitudes between 4% and 20%. Temperature was controlled at  $T = 20 \pm 0.2$  °C using a fluid thermostat.

### Oscillatory squeeze flow

Oscillatory squeeze flow experiments were performed using a piezo-driven axial vibrator (Crassous et al. 2005; Kirschenmann 2003) customized at the Institute for

Dynamic Material Testing (Ulm, Germany). In these experiments, the sample is placed into a gap between two stainless steel plates. The lower one is supported by a thin-walled quadratic copper tube carrying the piezo elements which exert the vibrational motion and pick-up the response signal. This lower part of the device is surrounded by a double-walled cylinder allowing for circulation of a thermostating fluid, and the sample temperature is controlled with an accuracy of  $\pm 0.1$  °C. The upper boundary of the gap is a thick metal lid, which provides complete sealing of the fluid. The instrument operates at a constant force amplitude, and from the ratio of the dynamic displacement of the lower plate (amplitude  $\sim 5$  nm) with and without fluid, the complex squeeze stiffness  $K^*$  of the fluid is obtained which is directly related to the complex shear modulus  $G^*$  assuming no-slip boundary conditions (Kirschenmann 2003):

$$K^* = \frac{3\pi R^4}{2d^3} G^* \left/ \left( 1 + \frac{\rho\omega^2 d^2}{10G^*} + \dots \right) \right. \quad (1)$$

where  $\rho$  is the fluid density,  $R$  (here 10 mm) is the radius, and  $d$  is the height of the gap. The denominator in Eq. 1 is a series expansion taking into account the inertia of the fluid in the gap. The determination of  $G^*$  strongly depends on the exact knowledge of  $d$ , which is determined by calibration using Newtonian liquids with viscosities between 1 and 2,000 mPa s. Gap heights between 15 and 100  $\mu\text{m}$  have been used here. Additional contributions of finite compressibility of the fluid can be safely neglected for the soft ( $G^* < 1,000$  Pa) polymer solutions investigated here, but samples have to be degassed carefully in order to avoid artificial compressibility from entrapped air. Moduli  $G'$  or  $G''$  in the range from 0.1 Pa to 10 kPa are accessible with the set-up described here.

### Capillary break-up extensional rheometry

In a CaBER experiment (Bazilevskii et al. 2001; Entov and Hinch 1997), a fluid drop is placed between two plates and subsequently exposed to an extensional step strain thus forming a liquid filament. A CaBER 1 (Thermo Electron) extensional rheometer was used here, equipped with plates of diameter  $d_c = 6$  mm. Plate separation was changed from  $L_{\text{ini}} = 6$  mm to  $L_{\text{fin}} = 16$  mm within 40 ms. This choice of parameters ensured that the initial filament diameter directly after the plate separation stops was always around 1–1.5 mm for the fluids investigated here, and thus,

capillary forces dominate over gravitational forces<sup>1</sup> and the subsequent necking of that liquid bridge is controlled by the balance of capillary and viscoelastic forces. The only measured quantity during filament necking is the change in the midpoint diameter  $D(t)$  with time, which is monitored using a laser micrometer. Deformation of a fluid element at the axial midplane of the bridge is purely uniaxial. Large extensional strains are attained as filament thins and finally breaks. The theoretical basis for the capillary thinning of fluid filaments has been discussed thoroughly (Entov and Hinch 1997). Having only the change in filament diameter as a function of time,  $D(t)$ , strain rate  $\dot{\epsilon}$ , tensile stress  $\tau_E$  and apparent extensional viscosity  $\eta_E$  can be calculated according to following simplified equations (McKinley and Tripathi 2000):

$$\dot{\epsilon} = -\frac{2}{D(t)} \frac{dD(t)}{dt} \quad (2)$$

$$\tau_E = \frac{2\sigma}{D(t)} \quad (3)$$

$$\eta_E = -\frac{\sigma}{\frac{dD(t)}{dt}} \quad (4)$$

Where  $\sigma$  is the surface tension of the fluid. The time directly after cessation of the motion of the plate is defined as  $t = 0$ , and the corresponding filament diameter  $D_0$  has been used to calculate the Hencky strain  $\epsilon(t)$ :

$$\epsilon(t) = 2 \ln \left( \frac{D_0}{D(t)} \right) \quad (5)$$

In addition to the determination of the midpoint diameter  $D(t)$ , the full filament shape during the thinning and necking process was monitored here for selected samples using a high-speed camera (Fastcam 1024 PCI Photron) taking 1,000 images/s at a resolution of  $1,024 \times 1,024$  pixel equipped with a macro zoom objective (Eneo Verifokal B 45 Z03 MV-MP, focal length 45–160 mm) and additional intermediate rings allowing for 0.3–1-fold magnification. Illumination was done with a white LED from the back. With this setup, filament thinning could be resolved down to  $10 \mu\text{m}$ . All CaBER experiments were performed at ambient temperature.

<sup>1</sup>This can be estimated by the so-called Bond number  $\text{Bo} = \rho g D(t)^2 / 4\sigma$  (see, e.g., Anna and McKinley 2001) with the acceleration of gravity  $g$ ,  $\text{Bo} < 0.2$  for a filament diameter of 1.5 mm,  $\sigma = 35 \text{ mN/m}$ , and  $\rho = 1,000 \text{ kg/m}^3$ .

## Results and discussion

### Shear rheology

We have prepared aqueous solutions of Sterocoll FD with concentrations of 0.7–5% and different pH values between 6.5 and 9.5. Viscosity of these solutions exhibits a maximum in the pH range around 8–9, and the results presented below focus on this pH range, which is also typical for many technical applications of such thickeners.

The linear viscoelastic properties of the solutions have been characterized using small amplitude oscillatory shear and squeeze flow thus covering a frequency range of about seven decades. The results for solutions with different polymer concentrations at pH = 8 are shown in Fig. 1a, b. This is the first analysis of the linear viscoelastic relaxation of ASE-type thickener solutions in such a broad frequency range, which allows for a robust comparison to model predictions.

All  $G'$ ,  $G''$  data show the same pattern, at low frequencies a terminal relaxation regime is found with  $G' \sim \omega^2$  and  $G'' \sim \omega$ , which switches over to a scaling regime covering more than four decades on the frequency axis. For both moduli, the same scaling exponent is found, which varies between 0.585 and 0.6 for the different solutions. This is the characteristic Zimm relaxation behavior and no crossover in  $G'$  and  $G''$  is observed. This important finding clearly reveals that despite the polymers' high molecular weight entanglements do not contribute to the stress relaxation of these solutions even at concentrations well above the overlap concentration  $c^*$ , and particularly also above typical concentrations at which these thickeners are used in commercial formulations. We estimate  $c^* \approx 1 / \sqrt{N} \approx 0.1\%$ , where  $N$  is the degree of polymerization of the aggregates, and according to scaling theory onset of entanglement is expected to occur around  $10c^*$  for polyelectrolytes in solutions of high ionic strength (Dobrynin et al. 1996) similar as for neutral polymers. Here entanglements are not observed even at higher concentrations, and we assume this is due to intra- and intermolecular “sticky” contacts among hydrophobic EA sequences within the aggregates.

For a quantitative analysis of our data,  $G'$  and  $G''$  were fitted using the relaxation function from the Zimm theory (Rubinstein and Colby 2003):

$$G(t) = \frac{\eta_s}{\lambda_0} \phi \left( \frac{t}{\lambda_0} \right)^{-1/3\nu} \exp \left( -\frac{t}{\lambda_z} \right) \quad (6a)$$

where  $\eta_s$  is the solvent viscosity and  $\phi$  the volume fraction of the polymer. The dynamic mechanical moduli

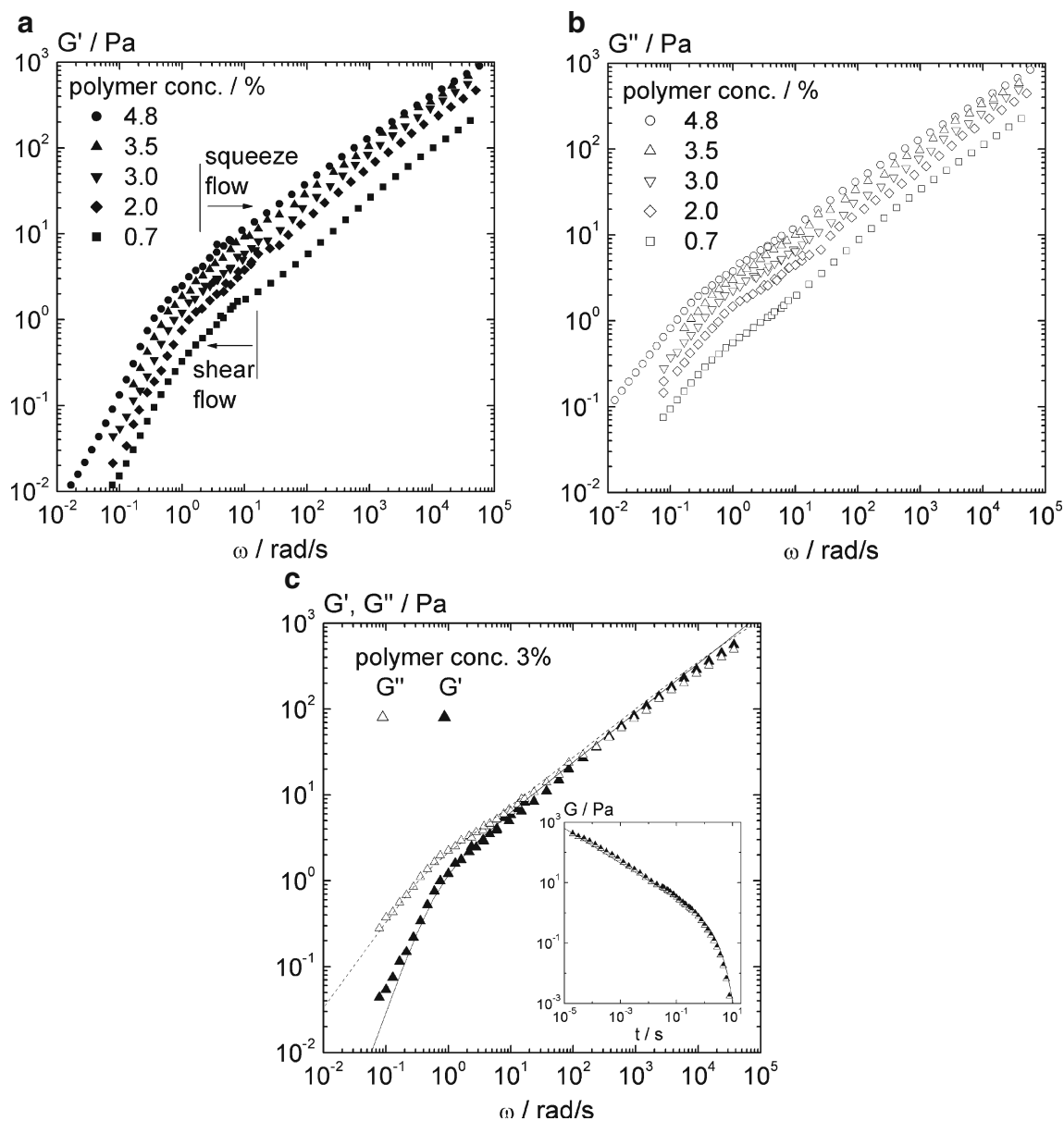


**Fig. 1** **a** Storage modulus  $G'$  vs. angular frequency for Sterocoll FD solutions with different polymer concentrations at  $pH = 8$ . The frequency ranges in which data have been obtained by oscillatory shear and squeeze flow, respectively, are indicated by arrows. **b** Loss modulus  $G''$  vs. angular frequency for Sterocoll FD solutions with different polymer concentrations at  $pH = 8$ .

**c** Storage and loss modulus  $G'$  and  $G''$  vs. angular frequency for a Sterocoll FD solution with polymer concentration 3 vol% at  $pH = 8$ . Lines: Fit of the Zimm model to the experimental  $G'$  (solid lines) and  $G''$  (dashed lines) data (for fit parameters see Table 1). Insert: Shear modulus  $G(t)$  used to fit the Zimm model to the experimental  $G'$  and  $G''$  data according to Eqs. 6a and 6b

can be calculated from this relaxation spectrum using the Ferry's relations (Ferry 1980):

$$G'(\omega) = \omega \int_0^{\infty} G(t) \sin(\omega \cdot t) dt$$

$$G''(\omega) = \omega \int_0^{\infty} G(t) \cos(\omega \cdot t) dt \quad (6b)$$

To enhance the efficiency and accuracy of the integral calculation, a finite element method introduced by Nobile and Cocchini (2001) was used to calculate  $G'(\omega)$  and  $G''(\omega)$ .

From a fit of Eqs. 6a and 6b to the experimental data, we determine the characteristic longest and shortest relaxation times  $\lambda_z$  and  $\lambda_0$  of the representative Zimm chain as well as the scaling exponent  $\nu$ .

**Table 1** Zimm analysis of the linear viscoelastic response of aqueous Sterocoll FD solutions of various polymer concentrations  $\phi$  at pH = 8

$\phi/\%$	$\eta_s/\text{mPa s}$	$\lambda_z/\text{s}$	$\lambda_0/10^{-10} \text{ s}$	$N_{\text{app}}/10^6$	$b/\text{\AA}$	$\nu$
0.7	1.0	$2.2 \pm 0.2$	$0.11 \pm 0.02$	$2.75 \pm 0.28$	$3.6 \pm 0.5$	$0.585 \pm 0.01$
2.0	1.0	$1.2 \pm 0.1$	$0.24 \pm 0.05$	$1.25 \pm 0.13$	$4.6 \pm 0.5$	$0.585 \pm 0.01$
3.0	1.0	$1.0 \pm 0.1$	$0.29 \pm 0.06$	$1.01 \pm 0.10$	$4.9 \pm 0.5$	$0.585 \pm 0.01$
3.5	1.0	$1.0 \pm 0.1$	$0.31 \pm 0.06$	$0.94 \pm 0.09$	$5.0 \pm 0.5$	$0.585 \pm 0.01$
4.8	1.0	$4.0 \pm 0.2$	$0.40 \pm 0.08$	$1.07 \pm 0.11$	$5.5 \pm 0.5$	$0.608 \pm 0.01$

The solvent viscosity given in the table was used as input parameter for the analysis of the  $G'$ ,  $G''$  data. Error margins given in the table are due to the uncertainty in reproducibility of shear modulus measurements and the corresponding error propagation when calculating the fit parameters and related quantities. The relative error in  $G'$  and  $G''$  is estimated to be 10%.

The shortest relaxation time  $\lambda_0$  is related to the length of a Kuhn segment  $b$  according to

$$b^3 = k_B T \frac{\lambda_0}{\eta_s} \quad (7)$$

and from the ratio of  $\tau_0$  and  $\tau_z$  we get the number of Kuhn segments  $N_{\text{app}}$ :

$$N_{\text{app}} = \left( \frac{\lambda_z}{\lambda_0} \right)^{1/3 \nu} \quad (8)$$

Of course, these are apparent values, because our analysis is based on the simplified Zimm model originally developed for linear polymer chains in dilute solutions, but here we are only interested in relative changes of  $b$  and  $N_{\text{app}}$  with changing solvent quality or polymer concentration.

The values for  $\lambda_0$ ,  $\lambda_z$ ,  $\nu$ ,  $N_{\text{app}}$ , and  $b$  determined for solutions with different polymer concentrations adjusted to pH = 8 are listed in Table 1. The exponent  $\nu = 0.585 \pm 0.01$  is as expected from the Zimm model for polymers in good solvents. The Kuhn length  $b$  is also essentially independent of concentration and varies between  $4.6 \pm 0.5$  and  $5.5 \pm 0.5 \text{ \AA}$ , and only at  $\phi = 0.7\%$  a slightly lower value of  $3.6 \pm 0.5 \text{ \AA}$  is found. From the bond length and angles of an average monomer unit we calculate that a Kuhn element represents 2–3 physical monomer units with an average  $M_w$  of 96 g/mol for a 1:1 MAA/EA copolymer composition. The Kuhn length  $b$  is calculated from the shortest measured relaxation time, which is determined by local displacements of short chain segments, and hence, it can be assumed that this quantity is hardly affected by interactions among single chains or aggregates. Therefore, we think it is justified to compare our data with independent results for pure poly(MAA) obtained from X-ray scattering and atomic force microscopy. For pure PMAA in aqueous solution, values for  $b$  in the range of 6–8  $\text{\AA}$  are reported in the literature in a broad range of degree of ionization and across the transition from contracted to expanded

random coil configuration (Muroga et al. 1999; Ortiz and Hadziioannou 1999). Finally,  $N_{\text{app}}$  and hence the product  $N_{\text{app}} \cdot b$  is independent of concentration, suggesting that the aggregate size is roughly independent of concentration.

In Fig. 2, we show the zero shear viscosity  $\eta_0$  for two dilution series adjusted to pH = 8 and pH = 9, respectively. At pH = 9, the viscosity is slightly lower than at pH = 8, but in both cases  $\eta_0$  increases only weakly with concentration and a power law dependence  $\eta_0 \sim \phi^{1.25 \pm 0.1}$  is found at concentrations  $\phi > 1\%$ . This is in excellent agreement with predictions for unentangled, semidilute solutions of neutral polymers (Colby et al. 1994) and polyelectrolytes in the high-salt limit (Dobrynin et al. 1996). The ionic strength of the solutions investigated here has not been controlled

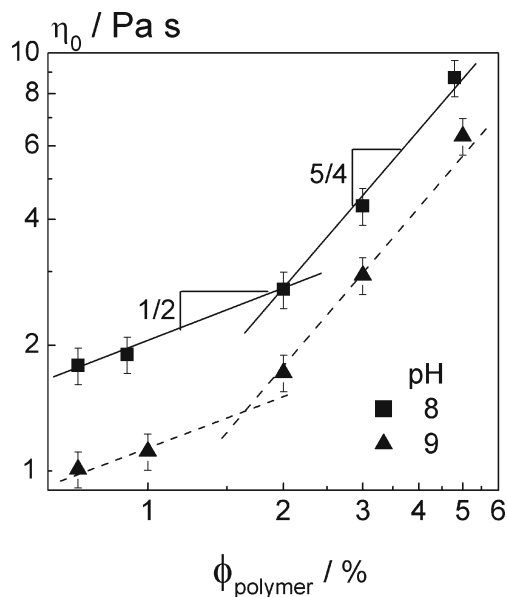
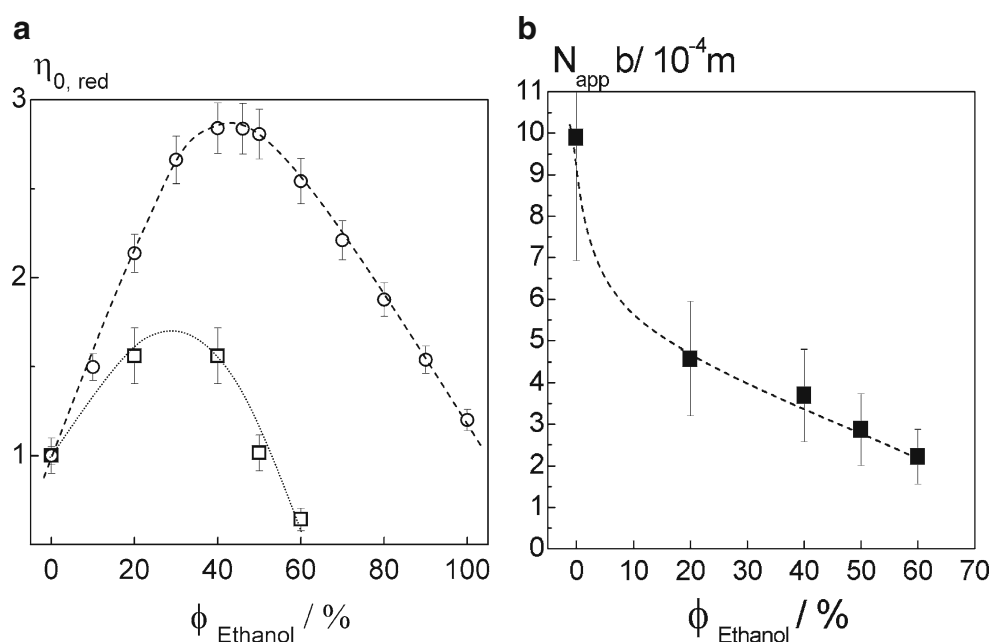


**Fig. 2** Zero shear viscosity as a function of polymer concentration for two different pH values. Error bars refer to the standard deviation of results from five measurements on different samples from the same batch

**Fig. 3 a** Reduced zero shear viscosity  $\eta_0$  vs. ethanol content  $\phi_{\text{Ethanol}}$  of the solvent mixture. *Circles*: pure solvent, *squares*: solutions with 0.7% polymer concentration but different solvent compositions. Data are normalized to water viscosity in the case of the pure solvent, for the solution to the viscosity of the solution in pure water. *Error bars* refer to the standard deviation of results from five measurements on different samples from the same batch. **b** Apparent degree of polymerization  $N_{\text{app}}$  times Kuhn segment length  $b$  vs. ethanol content  $\phi_{\text{Ethanol}}$  in the solvent mixture. *Line* is to guide the eye. For error bars, see Table 2



explicitly, but electrical conductivity varies from 2 to 10 mS/cm as  $\phi$  increases from 1% to 5%, indicating the high ionic strength of the solutions, which is due to the ions introduced during neutralization. Ionic strength decreases with decreasing polymer concentration since less NaOH is needed for neutralization; accordingly, a weaker concentration dependence of viscosity is observed approaching  $\eta_0 \sim \phi^{0.5}$  as expected for polyelectrolytes in the low-salt limit (Fuoss 1951; Dobrynin et al. 1996). Moreover, it is worth noting that the steady shear viscosity of solutions of Sterocoll FD is similar to that of solutions of linear acrylic acid homopolymers with about 50 times lower average molecular weight compared at similar polymer concentration and pH.<sup>2</sup> This also indicates a compact structure of the aggregates, which is presumably the reason for the absence of entanglements.

An appropriate means to vary solvent quality and hence the aggregation behavior of the copolymer is to add ethanol as a co-solvent to the polymer solutions. In Fig. 3a, we compare the corresponding  $\eta_0$  and in Fig. 3b the values of the product  $N_{\text{app}} \cdot b$  for a mixing series with 0.7% polymer concentration (Table 2). It is well known that ethanol–water mixtures exhibit a distinct maximum in viscosity at a mixing ratio of about 1:1, which is due to structure formation based on H-bonds. A similar behavior would be

expected for the corresponding polymer solutions if they were ideal solutions, since then solvent viscosity should be a constant pre-factor of the solution viscosity. In contrast, we observe that the viscosity maximum is less pronounced and occurs at lower ethanol content as compared to the pure ethanol–water mixture. At ethanol fractions beyond 0.5, the viscosity decreases even below that of the solution in pure water. But at an ethanol content beyond 0.6, the solutions get turbid and phase separate. This can be interpreted as follows: at low ethanol concentrations, aggregates partly break due to an increased solubility of the EA groups, and this counteracts the increase of the solvent viscosity and hence the viscosity maximum is less pronounced compared to the solvent mixture. Furthermore, the solubility of the MAA groups decreases with increasing ethanol content; thus, the polymer coils shrink and this additionally contributes to the reduction of viscosity. At high enough ethanol concentrations, this effect makes the copolymer insoluble, and thus the solution gets turbid, finally leading to phase separation. Zimm analysis shows that the product  $N_{\text{app}} \cdot b$ , which is a measure of the molecular weight of the aggregates, decreases monotonically with increasing ethanol content and thus directly shows the break-up of aggregates, which is attributed to the enhanced solubility of EA. This result is in line with the reduction of molecular weight observed in field flow fractionation experiments at much lower polymer concentrations, when replacing water by ethanol as a solvent.

<sup>2</sup>Private communication Y. Matter, BASF SE, ISIS Laboratory, Straßbourg.

**Table 2** Zimm analysis of the linear viscoelastic response of Sterocoll FD ( $\phi = 0.7\%$ ) dissolved in water–ethanol mixtures with different ethanol concentrations  $\phi_{\text{Ethanol}}$ 

$\phi_{\text{Ethanol}}/\%$	$\eta_s/\text{mPa s}$	$\lambda_z/\text{s}$	$\lambda_0/10^{-10} \text{ s}$	$N_{\text{app}}/10^6$	$b/\text{\AA}$	$\nu$
0	1.0	$2.2 \pm 0.2$	$0.11 \pm 0.02$	$2.75 \pm 0.28$	$3.6 \pm 0.5$	$0.585 \pm 0.01$
20	2.1	$1.8 \pm 0.2$	$0.60 \pm 0.02$	$0.93 \pm 0.09$	$4.9 \pm 0.5$	$0.585 \pm 0.01$
40	2.8	$1.8 \pm 0.2$	$1.00 \pm 0.20$	$0.70 \pm 0.07$	$5.3 \pm 0.5$	$0.585 \pm 0.01$
50	2.8	$1.8 \pm 0.2$	$2.80 \pm 0.28$	$0.39 \pm 0.04$	$7.4 \pm 0.5$	$0.585 \pm 0.01$
60	2.5	$1.4 \pm 0.2$	$5.20 \pm 0.52$	$0.24 \pm 0.02$	$9.4 \pm 0.5$	$0.585 \pm 0.01$

The solvent viscosity given in the table was used as input parameter for the analysis of the  $G'$ ,  $G''$  data. For error margins, see Table 1.

## Extensional rheology

The extensional flow properties of the thickener solutions have been characterized using the CaBER technique. In Fig. 4, the time dependence of the normalized midpoint diameter is shown for three different polymer concentrations between 0.7% and 1%. The difference in the initial diameter decay is not very pronounced, but the diameter at failure strongly decreases and filament lifetime increases with increasing polymer concentration. Moreover, high-speed imaging reveals distinct differences in break-up mechanisms, as shown in Fig. 5. At 0.7% polymer concentration, filament break-up occurs within 20 ms after the motion of the upper plate has stopped. In this short period of time, no homogenous cylindrical fluid filament is formed. The liquid bridge is belly-shaped and break-up seems to be driven by inertia and gravity. At polymer concentrations  $\geq 0.9\%$ , cylindrical fluid filaments are formed quickly and thin homogeneously. For the solution with 0.9% polymer content, a beads-on-a-string instability (Goldin et al. 1969; Clasen et al. 2006a, b; Wagner et al. 2005) occurs at a filament diameter of about 60  $\mu\text{m}$ , shortly

before the filament breaks. Similar phenomena have been observed for low viscosity, weakly elastic, aqueous solutions of high molecular weight polyethylene oxide (PEO; Oliveira et al. 2006). At all higher concentrations, filaments thin uniformly until they finally vanish. There is no indication of any filament instability or inhomogeneity in deformation within the optical resolution of our set-up. Figure 6 shows the evolution of the midpoint diameter for polymer concentrations  $\geq 1\%$ . An exponential decay of the filament diameter is observed over an extended period of time and  $D(t)/D_0$  can be described as:

$$D(t)/D_0 = \exp\left(-t/3\lambda_E\right) \quad (9)$$

The characteristic relaxation time  $\lambda_E$  is directly related to the strain rate  $\dot{\epsilon} = 2/3\lambda_E$ , which is constant in this regime (cf. Eq. 2). Furthermore, this behavior corresponds to an exponential growth of the tensile stress (cf. Eq. 7). In the terminal regime of the filament-thinning process, the diameter decreases faster than expected from a single exponential decay, resulting in a downward curvature of the  $D(t)/D_0$  vs. time curves in the semilog plot. The described behavior is typical for weakly elastic polymer solutions. It has been observed, e.g., for polyacrylamide solutions (Stelter et al. 2002), polystyrene Boger fluids (Anna and McKinley 2001), or PEO solutions (Oliveira et al. 2006) and is generally attributed to the strain hardening of these solutions related to the extension of polymer coils. The rapid filament decay in the terminal regime is generally attributed to the finite extensibility of the polymer chains (Clasen et al. 2006a, b).

Here we find that the maximum Hencky strain  $\epsilon_{\text{max}}$  at which the filaments break, and hence filament lifetime increase substantially with increasing polymer concentration. For further numerical analysis of the results, we fit a power law to the  $D(t)/D_0$  data and then we calculate  $\dot{\epsilon}$  and  $\eta_{E,\text{app}}$  analytically according to Eqs. 2 and 8. This avoids large scatter in results, which would be inferred from calculating the derivative of  $D(t)$  numerically. For the experimental data presented in

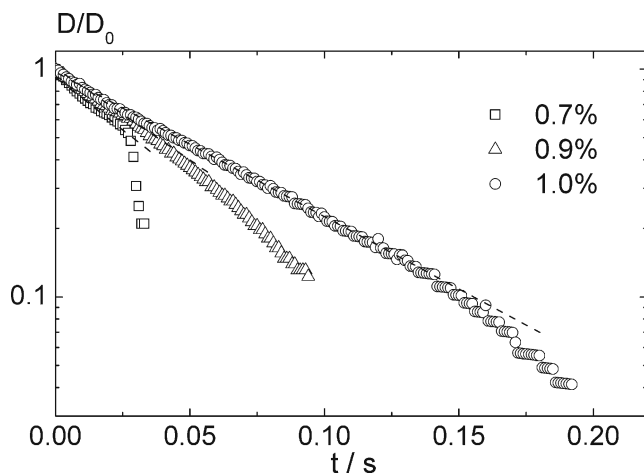


**Fig. 4** CaBER experiments: reduced filament midpoint diameter for solutions with different polymer concentrations at pH = 8. Dashed lines indicate initial slope of the respective data

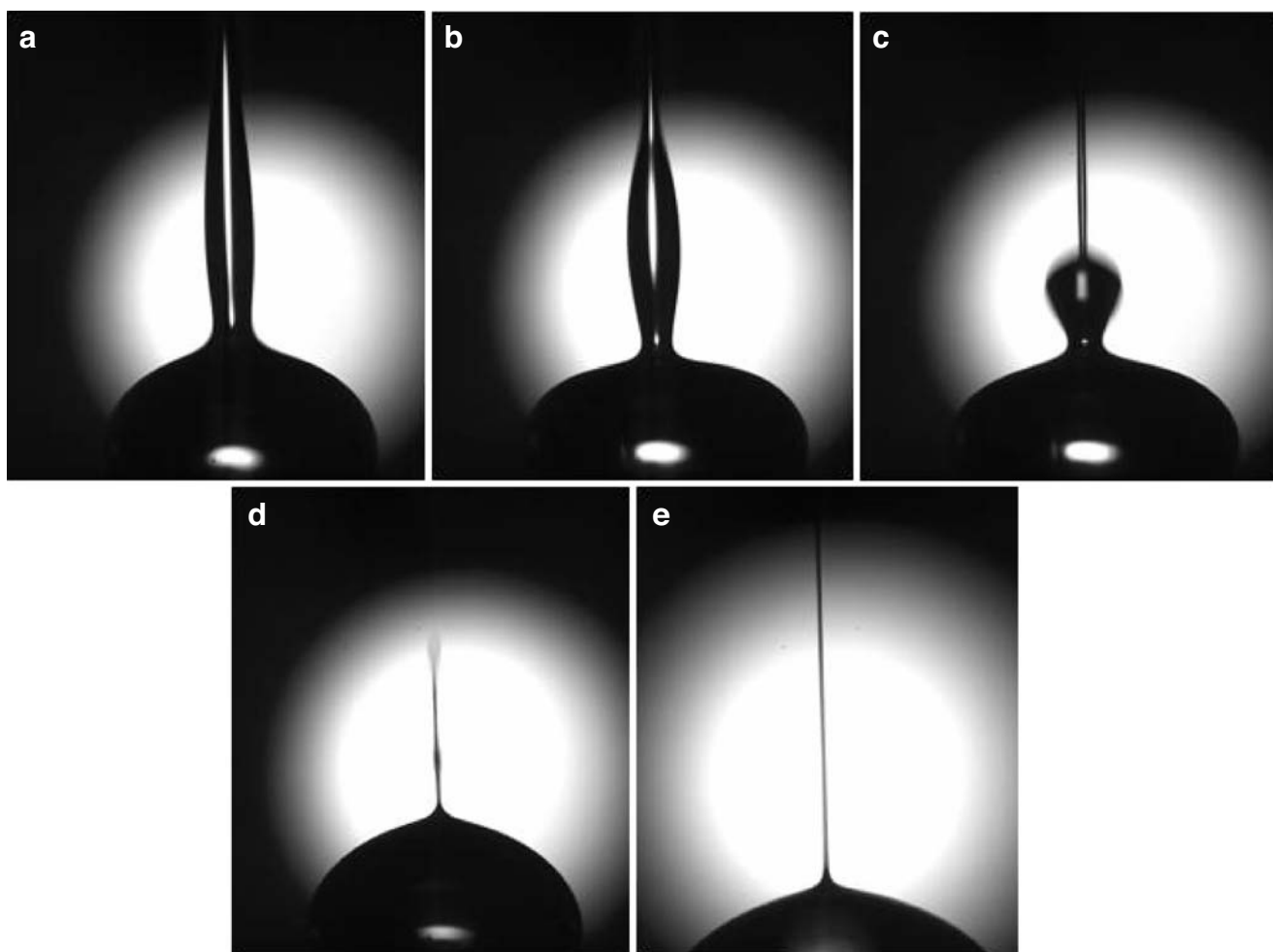


**Fig. 5** **a–e** Images of filaments from solutions with different polymer concentrations at pH = 8. **a–c** Taken after 27, 29, and 31 ms for polymer concentration 0.7%. **d** Last image before

failure ( $t = 94$  ms) for polymer concentration 0.9%. **e** Last image before failure ( $t = 197$  ms) for polymer concentration 1.0%

Fig. 6, this is shown in Fig. 7a, b. The self-selected strain rates in the CaBER experiments decrease with increasing polymer concentration and are in the range  $1\text{--}20\text{ s}^{-1}$ . For each concentration, the strain rate increases slightly with increasing total strain, but not more than 50% even up to Hencky strains of about 5. The ratios of the initial values of  $\eta_{E,\text{app}}$  and the zero shear viscosity for the different concentrations are between 1 and 2 and are thus slightly lower than the value of 3, which is expected in the limit of linear response. However, severe strain hardening is observed for all solutions. At the highest polymer concentration, the apparent extensional viscosity increases exponentially almost until failure at  $\varepsilon_{\text{max}} = 7.7$ . For lower concentrations, deviations from the exponential growth behavior occur around  $\varepsilon \approx 4$  and  $\eta_{E,\text{app}}$  seems to level off at higher strain, but this is related to the non-constant strain rate. Filament thinning and break-up results are very similar

at pH = 8, but at a slightly higher viscosity level. The corresponding values for the ratio  $\eta_{E,\text{app}}(t = 0)/\eta_0$  and  $\varepsilon_{\text{max}}$  are shown in Fig. 8.

A comparison of characteristic relaxation times in shear and extensional flow is shown in Fig. 9 for both concentration series at pH = 8 and pH = 9. Here we have calculated the longest relaxation time in shear  $\lambda_S$  according to:

$$\lambda_S = \lim_{\omega \rightarrow 0} \frac{G'}{G''\omega} \quad (10)$$

It is interesting to note that the relaxation times calculated in this way are systematically lower than those from Zimm analysis. At all investigated concentrations,  $\lambda_E$  is at least a factor of 10 lower than  $\lambda_S$ . At the lowest concentrations the difference is even more pronounced, but in these cases the short extension relaxation time is attributed to the occurrence of flow instabilities. At

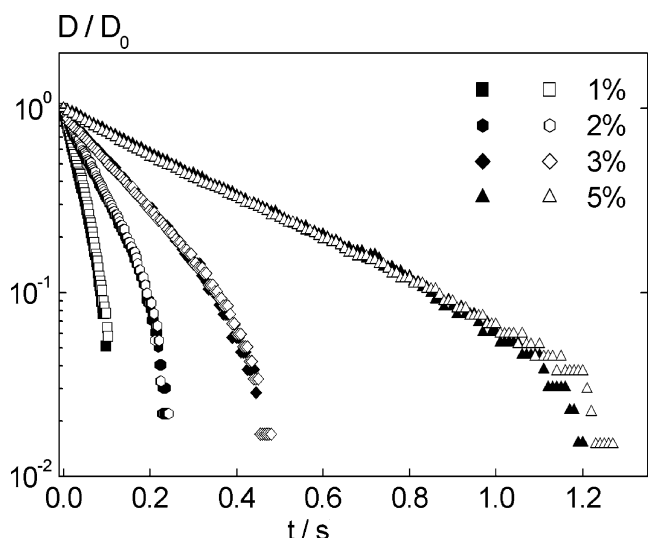


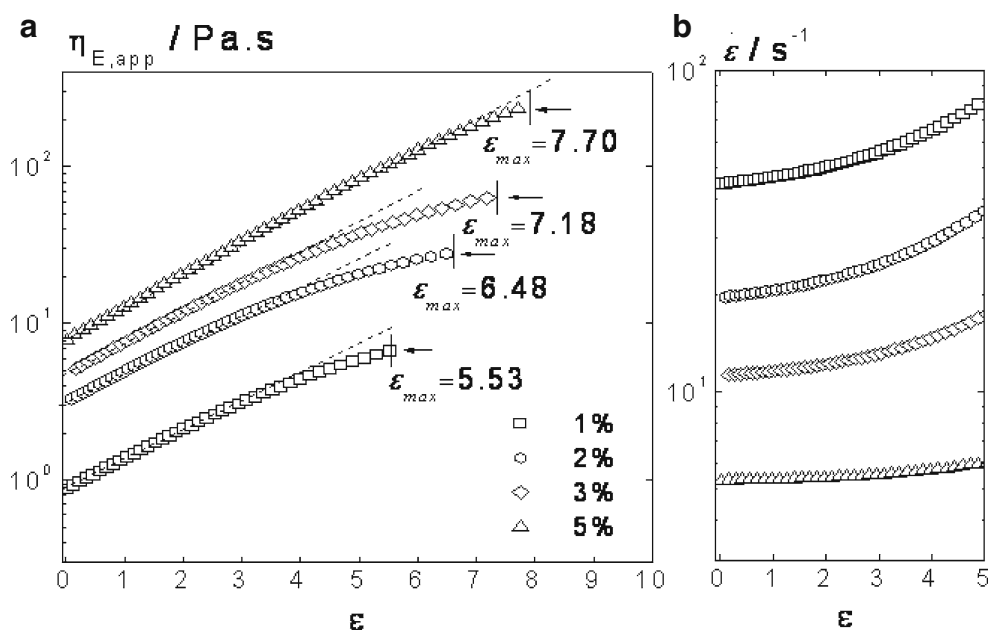
**Fig. 6** CaBER experiments: reduced filament midpoint diameter for solutions with different polymer concentrations at  $pH = 9$ . Open and closed symbols mark two different measurements visualizing the reproducibility of the experiment

high enough concentrations, filament thinning is dominated by viscoelastic response of the polymer chains and their unraveling,  $\lambda_E$  exhibits the same concentration dependence as  $\lambda_S$ , but still  $\lambda_E/\lambda_S \approx 0.1$ . To our knowledge, this is the lowest  $\lambda_E/\lambda_S$  ratio reported so far. For solutions of linear, flexible polymers like PS and PEO, it has been found that  $\lambda_E/\lambda_S \approx 1$  (Anna and McKinely 2001; Oliveira et al. 2006). In the case of entangled wormlike micellar solutions,  $\lambda_E/\lambda_S \approx 1/3$  has been reported, and this low value has been attributed to the dynamic nature of breaking and reforming micelles,

which are also termed living polymers (Yesilata et al. 2006). Two mechanisms are considered to cause the distinct behavior of the thickener solutions observed here. Firstly, it could be the consequence of a partial break-up of molecular aggregates. These aggregates which determine the shear viscosity cannot withstand the strong elongational flow and thus cannot stabilize the filament in a CaBER experiment. For comparison, Tan et al. (2000) also attribute a decrease in the extensional viscosity observed for hydrophobically modified HASE-type acrylate thickener solutions at high elongation rates to a break-up of intermolecular clusters in strong extensional flows. Secondly, it could be due to the rigidity of the aggregates. These aggregates are assumed to be less deformable than linear, flexible polymers, because of inter- and intramolecular “sticky” contacts among EA sequences, and hence cannot contribute much to the elongational flow resistance. A lower elongational viscosity of rigid compared to flexible polymers has previously also been reported by Dexter (1996) and Stelter et al. (2002). The contribution of aggregate rigidity should partly scale out when  $\lambda_E/\lambda_S$  is discussed and moreover, strain hardening would hardly occur for only weakly deformable aggregates. Therefore, aggregate break-up seems to be more likely, but a final distinction between these two possible mechanisms is not possible on the basis of the results obtained so far. This would require additional structural investigations under flow conditions, which are beyond the scope of this paper.

Figure 10 shows the time dependence of the midpoint diameter for solutions of 0.9% polymer in

**Fig. 7** Apparent extensional viscosity (a) and strain rate (b) vs. Hencky strain for solutions with different polymer concentrations at  $pH = 9$



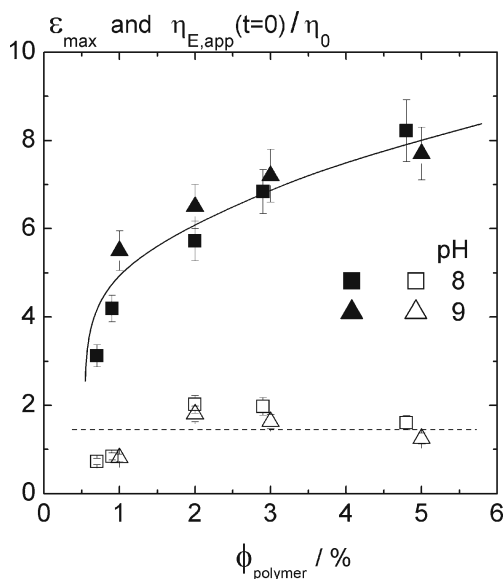


**Fig. 8** Hencky strain at failure (*closed symbols*) and ratio of initial elongational viscosity to zero shear viscosity (*open symbols*) vs. polymer concentration for solutions at pH = 8 and pH = 9. *Lines* are to guide the eye. *Error bars* refer to the standard deviation of results from five measurements on different samples from the same batch

different mixtures of water and ethanol as solvent. Filament thinning takes place nearly exponentially up to an ethanol content of 50%, and the characteristic relaxation time  $\lambda_E$  as well as the Hencky strain at failure  $\varepsilon_{\max}$

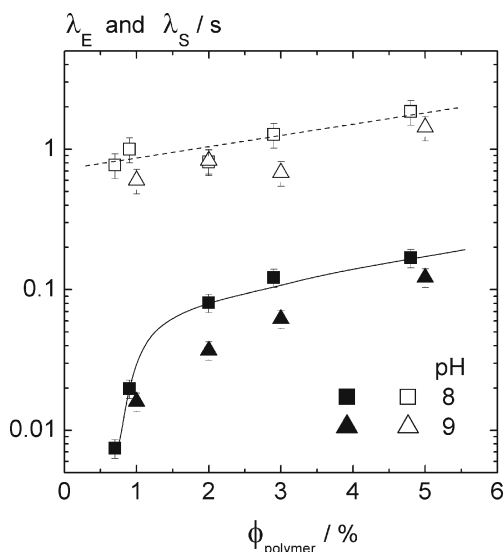


**Fig. 9** Characteristic relaxation time from shear (*open symbols*) and CaBER experiments (*closed symbols*) vs. polymer concentration at pH = 8 and pH = 9. *Lines* are to guide the eye. *Error bars* for  $\lambda_E$  refer to the standard deviation of results from five measurements on different samples from the same batch. *Error bars* for  $\lambda_S$  are calculated from the errors in determination of  $G'$  and  $G''$  (see Table 1)

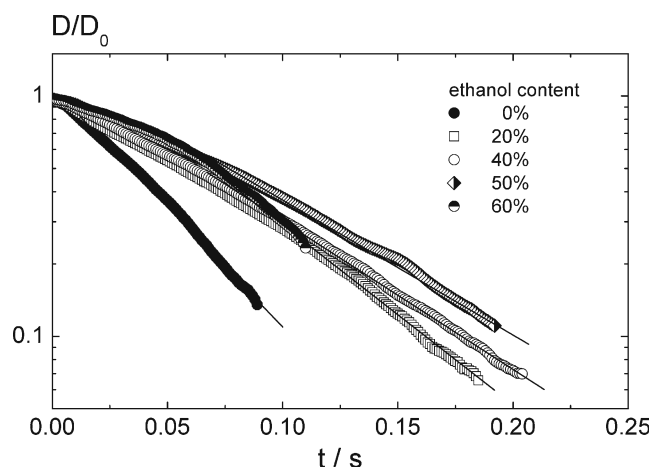


**Fig. 10** CaBER experiments: reduced filament midpoint diameter for solutions with different solvent compositions. The ethanol content varies as indicated in the legend. The polymer concentration is always 0.9% and pH = 9

increase with increasing ethanol content. At an ethanol concentration of 60%  $\varepsilon_{\max}$  decreases drastically, and in addition, the  $D(t)$  curve exhibits a pronounced downward curvature. At this ethanol concentration close to the solubility limit as well as for the solution in pure water, filament failure is finally controlled by a beads-on-a-string instability, which occurs due to the low viscosity of these samples. At intermediate ethanol concentrations, filaments thin homogeneously until they break at about 50–60  $\mu\text{m}$ . The characteristic relaxation times from oscillatory shear and CaBER experiments are compared in Fig. 11. The shear relaxation time goes through a shallow maximum, similar to the zero shear viscosity, while the CaBER relaxation time increases by a factor of two when ethanol content is increased up to 50%. At this ethanol concentration, the ratio  $\lambda_E/\lambda_S$  is almost three times higher than for the solution in pure water. No elongational relaxation time was determined for the solution with 60% ethanol content because of the non-exponential filament decay.

These observations can be rationalized as follows: The increasing relaxation time which corresponds to a decreasing strain rate is a consequence of the decreasing tensile stress. The surface tension  $\sigma$  decreases from 35 mN/m for the solution in pure water to 29 mN/m for the solution with 50% ethanol content.<sup>3</sup> On the other hand, the increasing solvent quality reduces the size of aggregates, which results in a reduction of  $\lambda_S$  as well

<sup>3</sup>It should be noted that the low  $\sigma$  value even for the pure aqueous solution is due to the presence of surfactants from the emulsion polymerization process.

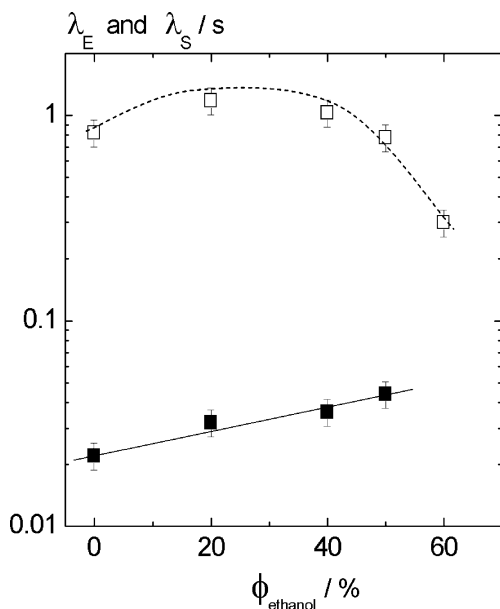


**Fig. 11** Characteristic relaxation time from shear (*open symbols*) and CaBER experiments (*closed symbols*) vs. ethanol concentration. The polymer concentration is always 0.9% and pH = 9. *Lines* are to guide the eye. *Error bars* for  $\lambda_E$  refer to the standard deviation of results from five measurements on different samples from the same batch. *Error bars* for  $\lambda_S$  are calculated from the errors in determination of  $G'$  and  $G''$  (see Table 1)

as an increase in  $\lambda_E/\lambda_S$  at ethanol fractions of 40%. In addition, also the number of “sticky” intramolecular contacts reduces with increasing solvent quality, and thus the chains or aggregates can be stretched to a higher extent in the extensional flow field and stabilize the filaments at higher  $\varepsilon$  (or lower diameter).

## Conclusion

Alkali-swellable acrylate thickeners are widely used in different applications like coatings, adhesives, or personal care products. Here we have used the commercial thickener Sterocoll FD as a model system for investigation of the molecular mechanisms controlling the thickening properties of this class of polymers. This polyelectrolyte is a statistical copolymer of methacrylic acid and ethylacrylate. These copolymers are known to form intermolecular aggregates in aqueous solution due to the hydrophobic nature of statistically occurring EA sequences. Neutralized aqueous solutions of this type of polymer are highly viscous, but weakly elastic at concentrations (0.5–5 wt.%) typically used in technical applications.

We have investigated shear as well as elongational flow properties of solutions in this range of polymer

concentrations to gain deeper insight into the dominating thickening mechanisms. Linear viscoelastic moduli  $G'$  and  $G''$  have been determined in a broad frequency range up to  $10^4$  rad/s employing oscillatory squeeze flow. Extensional flow behavior has been characterized using the CaBER technique including high-speed imaging for control of the homogeneity of deformation and the limits of filament stability.

Zero shear viscosity  $\eta_0$  is low and shear thinning is weak compared to the high molecular weight of the aggregates. Linear viscoelastic relaxation is described by classical Zimm theory up to frequencies of  $10^4$  rad/s and no crossover of  $G'$  and  $G''$  occurs, demonstrating that no entanglements are present in these solutions even at concentrations far above the critical overlap concentration. This is also confirmed by the characteristic concentration dependence of the zero shear viscosity  $\eta_0 \sim \phi^{1.25}$ . We attribute these findings to strong association within the aggregates. Our rheological investigations further reveal that these aggregates disintegrate if part of the solvent is replaced by ethanol. This is in agreement with field flow fractionation results obtained at much lower polymer concentrations.

At low polymer concentration and hence low solution viscosity, filament break-up in CaBER experiments is induced by beads-on-a-string instabilities. But at concentrations  $\geq 1\%$ , all solutions undergo uniform elongational deformation and show pronounced strain hardening at constant strain rate up to large Hencky strains, and  $\varepsilon_{\max}$  increases from 5.5 to 7.5 as polymer volume fraction  $\phi$  increases from 1% to 5%. Time evolution of the filament diameter is described by a single Maxwell model. The corresponding relaxation time  $\lambda_E$  is always at least one order of magnitude lower than the longest shear relaxation time  $\lambda_S$ . Thus we conclude that the aggregates, which control shear rheology, cannot contribute to the elongational viscosity. This is could either be due to the high rigidity of the aggregates caused by sticky contacts among hydrophobic EA sequences within the aggregates or due to a disintegration of the aggregates in the strong extensional flow. The latter result is more likely, but a distinction between these mechanisms would require additional structural investigations. Aggregate molecular weight decreases with increasing solvent quality and accordingly the ratio of  $\lambda_E/\lambda_S$  increases upon partial replacement of water by ethanol. Furthermore, the number of “sticky” intramolecular contacts reduces with increasing solvent quality (ethanol content), and thus the chains or aggregates can be stretched to a higher extent in the extensional flow field and stabilize the filaments at higher  $\varepsilon$ .

Our investigations show that this type of alkali-swellaable thickener is especially advantageous for applications where a low elongational viscosity at a relatively high shear viscosity level is required. Variation of solvent quality can be used to tune the balance between shear and elongational flow resistance. This result may have a broader perspective beyond the class of acrylate thickeners, since it is known that many other polymers, especially biopolymers like starch or various cellulose derivatives, which are also frequently used as thickeners, dissolve incompletely and also form intermolecular aggregates in aqueous solutions (Schulz et al. 1998).

**Acknowledgements** We would like to thank Amit Kumar Raj and Chris Woodson for their help in sample preparation and performing CaBER experiments, Kerstin Frank is thanked for assistance in high-speed imaging of filament break-up, and Sven Machauer for performing FFF experiments. We appreciate the assistance of Oliver Arnolds in preparing the manuscript.

## References

- Abdala AA, Wu W, Olsen KR, Jenkins RD, Tonelli AE, Khan SA (2004) Solution rheology of hydrophobically modified associative polymers: effects of backbone composition and hydrophobe concentration. *J Rheol* 48:979–994
- Agarwal S, Gupta RK (2002) An innovative extensional viscometer for low-viscosity and low-elasticity liquids. *Rheol Acta* 45:456–460
- Anna S, McKinley GH (2001) Elasto-capillary thinning and breakup of model elastic liquids. *J Rheol* 45:115–138
- Bazilevskii AV, Entov VM, Rozhkov AN (2001) Breakup of an Oldroyd liquid bridge as a method for testing the rheological properties of polymer solutions. *Polym Sci Ser A* 43: 716–726
- Bhardwaj A, Richter D, Chellamuthu M, Rothstein JP (2007) The effect of pre-shear on the extensional rheology of worm-like micelle solutions. *Rheol Acta* 46:861–875
- Braun DB, Rosen MR (2000) *Rheology modifiers handbook, practical use & application*. William Andrew, Norwich, NY, US
- Chao KK, Child CA, Grens EA, Williams MC (1984) Antimisting action of polymeric additives in jet fuels. *AICHE J* 30: 111–120
- Clasen C, Eggers J, Fontelos MA, Li J, McKinley GH (2006a) The beads-on-string structure of viscoelastic threads. *J Fluid Mech* 556:283–308
- Clasen C, Plog JP, Kulicke WM, Owens M, Macosko C, Scriven LE, Verani M, McKinley GH (2006b) How dilute are dilute solutions in extensional flows. *J Rheol* 50:849–881
- Cölfen H, Antonietti M (2000) Field-flow fractionation techniques for polymer and colloid analysis. *Adv Polym Sci* 50:67–187
- Colby RH, Rubinstein M, Daoud M (1994) Hydrodynamics of polymer solutions via two-parameter scaling. *J Phys (Paris)* 4(8):1299–1310
- Crassous JJ, Régisser R, Ballauff M, Willenbacher N (2005) Characterization of the viscoelastic behavior of complex fluids using the piezoelectric axial vibrator. *J Rheol* 49: 851–863
- Dai S, Tam KC, Jenkins RD (2000) Aggregation behavior of methacrylic acid/ethyl acrylate copolymer in dilute solutions. *Eur Polym J* 36:2671–2677
- Dexter RW (1996) Measurement of extensional viscosity of polymer solutions and its effects on atomization from a spray nozzle. *At Sprays* 6:167–191
- Dobrynin AV, Colby RH, Rubinstein M (1996) Scaling theory of polyelectrolyte solutions. *Macromolecules* 28:1859–1871
- English RJ, Gulati HS, Jenkins RD, Khan S (1997) Solution rheology of hydrophobically modified alkali soluble associative polymers. *J Rheol* 41:427–444
- Entov VM, Hinch EJ (1997) Effect of a spectrum of relaxation times on the capillary thinning of a filament of elastic liquid. *J Non-Newton Fluid Mech* 72:31–53
- Ferguson J, Hudson NE, Odriozola MA (1997) The interpretation of transient extensional viscosity data. *J Non-Newton Fluid Mech* 68:241–257
- Fernando RH, Xing LL, and Glass JE (2000) Rheology parameters controlling spray atomization and roll misting behavior of waterborne coatings. *Prog Org Coat* 40:35–38
- Ferry JD (1980) *Viscoelastic properties of polymers*. Wiley, New York
- Fuoss RM (1951) Polyelectrolytes. *Discuss Faraday Soc* 11: 125–135
- Goldin M, Yerushalmi H, Pfeffer R, Shinnar R (1969) Breakup of a laminar capillary jet of a viscoelastic fluid. *J Fluid Mech* 38:689–711
- Giddings JC (1993) *Field-flow fractionation: analysis of macromolecular, colloidal, and particulate materials*. Science 260:1456–1465
- Hager O, Martin R (1957) Copolymer of acrylic acid ester, method of making, and use of said polymer to coat textile fabrics. US patent 3003987 and Martin and Hager (1957) Acrylic tetrapolymer and textiles coated with the same. US patent 3070561
- James DF, Yogachandran N, Roper JA III (2003) Fluid elasticity in extension, measured by a new technique, correlates with misting. In: 8th TAPPI advanced coating fundamentals symposium, Chicago, pp 166–171
- Kennedy JC, Meadows J, Williams P (1995) Shear and extensional viscosity characteristics of a series of hydrophobically associating polyelectrolytes. *J Chem Soc Faraday Trans* 91:911–916
- Kirschenmann L (2003) PhD Thesis Institut für Dynamische Materialprüfung, Universität Ulm
- Kokko A, Kuni S, Grankvist T (1999) The influence of elongational viscosity on coat weight in paperboard coating with a smooth rod. In: 6th TAPPI advanced coating fundamentals symposium, Toronto, pp 79–97
- Kumacheva E, Rharbi Y, Winnik MA, Guo L, Tam KC, Jenkins RD (1996) Fluorescence studies of an alkaline swellaable associative polymer in aqueous solution. *Langmuir* 12:182–186
- Macosko CW (1994) *Rheology principles, measurements and applications*. Wiley-VCH, New York
- McKinley GH, Tripathi A (2000) How to extract the Newtonian viscosity from capillary breakup measurements in a filament rheometer. *J Rheol* 44:653–670
- McKinley GH, Sridhar T (2002) Filament-stretching rheometry of complex fluids. *Annu Rev Fluid Mech* 34:375–415
- Miller E (1960) Mineral coated paper products and methods of making them. US patent 3081198
- Muroga Y, Yoshida T, Kawaguchi S (1999) Conformation of poly(methacrylic acid) in acidic aqueous solution studied by small angle X-ray scattering. *Biophys Chem* 81:45–57

- Ng SL, Mun RP, Boger DV, James DF (1996) Extensional viscosity measurements of dilute solutions of various polymers. *J Non-Newton Fluid Mech* 65:291–298
- Ng WK, Tam KC, Jenkins RD (2001) Rheological properties of methacrylic acid/ethyl acrylate copolymer: comparison between an unmodified and hydrophobically modified system. *Polymer* 42:249–259
- Nobile MR, Cocchini F (2001) Evaluation of molecular weight distribution from dynamic moduli. *Rheol Acta* 40:111–119
- Oliveira MSN, Yeh R, McKinley GH (2006) Iterated stretching, extensional rheology and formation of beads-on-a-string structures in polymer solutions. *J Non-Newton Fluid Mech* 137:137–148
- Ortiz C, Hadziioannou G (1999) Entropic elasticity of single polymer chains of poly(meth acrylic acid) measured by atomic force microscopy. *Macromolecules* 32(3):780–787
- Plog JP, Kulicke WM, Clasen C (2005) Influence of molar mass distribution on the elongational behavior of polymer solutions in capillary breakup. *Appl Rheol* 15:28–37
- Rubinstein M, Colby R (2003) *Polymer physics*. Oxford University Press, Oxford
- Schulz L, Burchard W, Donges R (1998) In: Heinze TJ, Glasser WG (eds) *Cellulose derivatives, modifications, characterization and nanostructures*. ACS Symp Ser, Vol 688, p. 218
- Siddiq M, Tam KC, Jenkins RD (1999) Dissolution behaviour of model alkali-soluble emulsion polymers: effects of molecular weights and ionic strength. *Colloid Polym Sci* 277:1172–1178
- Solomon MJ, Muller SJ (1996) The transient extensional behavior of polystyrene-based Boger fluids of varying solvent quality and molecular weight. *J Rheol* 40:837–856
- Stelter M, Brenn G, Yarin AL, Singh RP, Durst F (2000) Validation and application of a novel elongational device for polymer solutions. *J Rheol* 44:595–616.
- Stelter M, Brenn G, Yarin AL, Singh RP, Durst F (2002) Investigation of the elongational behavior of polymer solutions by means of an elongational rheometer. *J Rheol* 46:507–527
- Tan H, Tam KC, Tirtaamadja V, Jenkins RD, Bassett DR (2000) Extensional properties of model hydrophobically modified alkali-soluble associative (HASE) polymer solutions. *J Non-Newton Fluid Mech* 92:167–185
- Tripathi A, Tam KC, McKinley GH (2006) Rheology and dynamics of associative polymers in shear and extension: theory and experiments. *Macromolecules* 39:1981–1999
- Tuladhar TR, Mackley MR (2008) Filament stretching rheometry and break-up behaviour of low viscosity polymer solutions and inkjet fluids. *J Non-Newton Fluid Mech* 148:97–108
- Wagner C, Amarouchene Y, Bonn D, Eggers J (2005) Droplet detachment and bead formation in visco-elastic fluids. *Phys Rev Lett* 95:164504
- Wang C, Tam KC, Tan CB (2005) Dissolution and swelling behaviors of random and cross-linked methacrylic acid-ethyl acrylate copolymers. *Langmuir* 21:4191–4199
- Willenbacher N (2004) Elongational viscosity of aqueous thickener solutions from capillary break-up elongational rheometry (CaBER). *Proc XIVth Int Cong Rheol*, Seoul, S Korea
- Yesilata B, Clasen C, McKinley GH (2006) Nonlinear shear and extensional flow dynamics of wormlike surfactant solutions. *J Non-Newton Fluid Mech* 133:73–90